European Geosciences Union General Assembly 2012, Vienna, Austria, 22-29 April
Session AS2.2/OS5.3: Turbulence in the atmospheric and oceanic boundary layers, Vol. 14, EGU2012-12672

Statistical analysis of positively buoyant turbulent jets

Dimitriadis P. & Papanicolaou P., Department of Water Resources and Environmental Engineering, National Technical University of Athens
(www.itia.ntua.gr, pandim@itia.ntua.gr)

Abstract

The future aim of this work is to create a statistical model for positively buoyant turbulent jets. For this, a statistical analysis is presented here, of two-dimensional (2D) spatio-temporal temperature records, obtained from tracer concentration measurements on the plane of symmetry of vertical heated jet. Some of the statistical tools used in this analysis are the probability and probability density distributions, energy spectrum, climacograms and Hurst coefficient distribution, autocorrelation and structural functions. Moreover, the above measurements are compared with existing ones from the literature.

1. Introduction

Study of turbulent jets is motivated by engineering applications to several fields such as mixing ventilation, wastewater disposing, gaseous releases, aerodynamic noise. In this study, several statistical tools are presented and applied to laboratory spatio-temporal temperature records obtained at the plane of symmetry of a vertical buoyant jet. More specifically:

(a) The mean and root-mean square (RMS) spatial distributions are estimated throughout the 2D flow field in order to determine the symmetric axis of the jet as well as its RMS axes. Moreover, several spatial density distributions (SDD) are also being derived.

(b) Temporal cumulative probability (CPF) and probability density (PDF) functions are estimated in several locations along the jet-axis.

(c) Energy spectrums (ES) are calculated in several locations along the jet-axis with smoothing and non-smoothing techniques and their log-slope is compared with Kolmogorov's -5/3 one of the inertial scale of motion.

(d) Climacograms (Cl) are also derived along the jet-axis and the Hurst-Kolmogorov coefficient (HKc) is calculated and compared with theoretical values.

(e) Finally, the temporal autocorrelation function (ACF) and the corresponding structural one of the 2nd order (S2F) are again estimated along the jet-axis.

2. Experimental set-up and calibration

The application presented is based on an experiment of a heated vertical buoyant round jet held at the laboratory of Hydraulics at the NTUA. This experiment is based on a planar laser-induced fluorescence (PLIF) technique. First, the jet is dyed with rhodamine 6G (R6G) dye (with initial concentration C_o). A laser beam (at wavelength of 532 nm) is then converted to a thin laser light sheet via a rotating prism mirror and illuminates the jet flow field. R6G emits (yellow) light at 556 nm when is excited by the laser light making the flow field visible. Finally, the concentration of R6G can be estimated through visualization techniques and its light intensity I can be linked to the flow's concentration through Walker (1987) and Ferrier et al. (1993) analysis. C_o is taken ≈30μg/l, less than 50μg/l, as suggested by Ferrier et al., (1993) and laser attenuation coefficients are estimated as $\varepsilon_I = 3.3\ 10^{-5}$ l/μg/m (through R6G) and $\eta_{Iw} = 3.3\ 10^{-5}$ m^{-1} (through water).

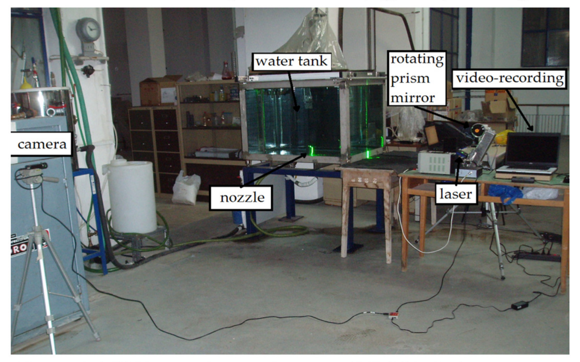

Figure 1: PLIF experimental set-up (NTUA, Laboratory of Hydraulics). The camera (for video tapping), nozzle, water-tank, rotating prism mirror, laser and video-recording (for video digitization) are shown.

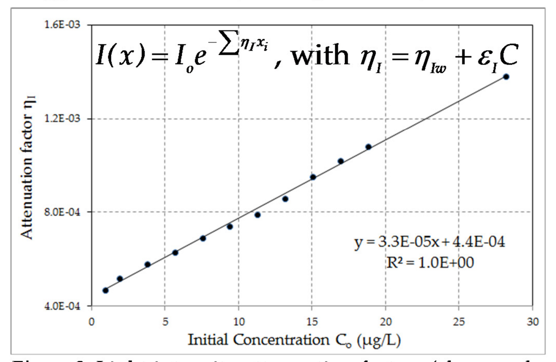

Figure 2: Light intensity attenuation factors (slope and intercept of the trend-line). Where C is the R6G concentration and x_i the distance the laser beam travels through the water-tank (from pixel i to i-1).

3. Data processing

- All the information concerning the experiment are gathered in figure 3.
- The image scale Sc and lens' distortion (pixel size variation along height) are estimated from a ruler placed on the nozzle.
- Noise from the camera (estimated via recording with the camera lens covered), background noise (estimated via recording with no jet discharge) and noise from slow motion of ambient water (observed from suspended particles) is estimated to be less than 1% (see P1, P2 in fig. 6).
- Totally, 3 locations are chosen along the jet-axis to apply the statistical tools described above. The first point (P1) is S1=5 cm away from the nozzle (close to the zone of flow establishment) and the other two (P2 and P3) within the zone of established flow (S2=15 and S3=25 cm away). All points lie within the jet-like area (momentum forces >> buoyancy forces), as Si/lm<1.

Co (μg/l)	28.6
SS (msec)	100
FR (fps)	20
Frames	10000
D (cm)	0.5
Q (ml/s)	18.6
Tjet (oC)	35.6
ρvjet (kg/m3)	994.0
Tam (oC)	16.9
ρvjet (kg/m3)	998.8
go'	4.8
M (cm^4/s^2)	1764.8
B(cm^4/s^3)	88.5
Re	6595
lq	0.44
lm	28.95
Ri	0.015

Figure 3: C_o, is the initial R6G concentration, SS is the camera's shutter speed, FR the camera's recording speed in frames per second, D is the nozzle diameter. Q, go', M, B, Re and Ri, are the initial discharge, the buoyancy acceleration, the jet specific momentum and the buoyancy flux, respectively. Tjet and Tam are the jet and ambient temperatures. ϱvjet and ϱvamb are the jet and ambient water densities, lq and lm characteristic length scale ($M^{3/4}B^{-1/2}$ and $QM^{-1/2}$).

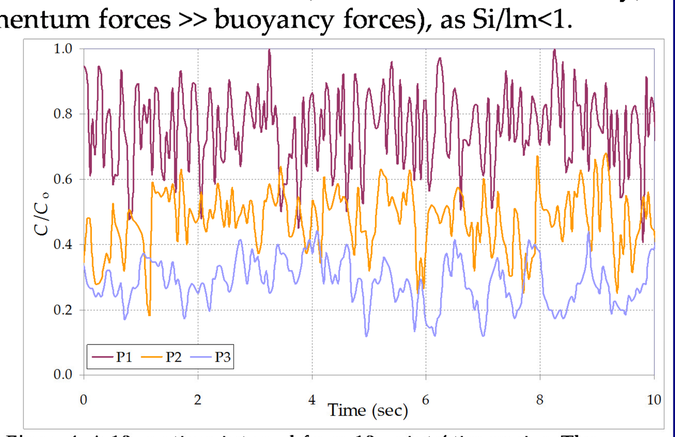

Figure 4: A 10 sec time interval from 10 points' timeseries. The number besides Pi (i 1 to 10) is the distance from the nozzle in cm.

4a. Time-averaged flow field

The estimated time-averaged distribution of the concentration as well as the SDD along the jet-axis and perpendicular to it, are presented below.

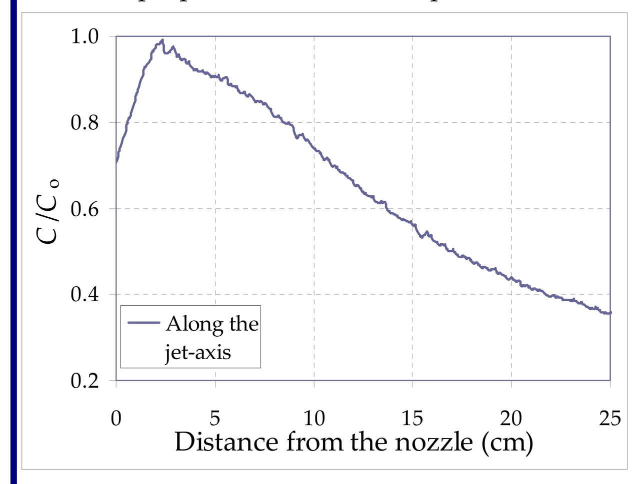

Figure 5a: Distribution of the concentration along the jet-axis.

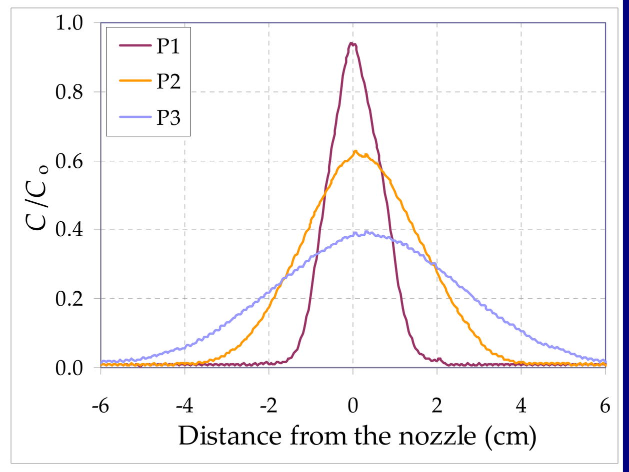

Figure 5b: Distribution of the concentration perpendicular to the jet-axis.

One can observe that the mean concentration is not constant within the ZFE (zone of flow establishment). A possible explanation could be that the initial concentration of R6G is high for the laser to pass through in a small area around the nozzle. The SSD type in the figure on the left seems to approximate the log-normal one. This agrees with many other records from experiments conducted with similar initial conditions and techniques, i.e. Papanicalou &List (1987).

4b. RMS flow field

The estimated RMS distribution of the concentration as well as the SDD along the jet-axis and perpendicular to it, are presented below.

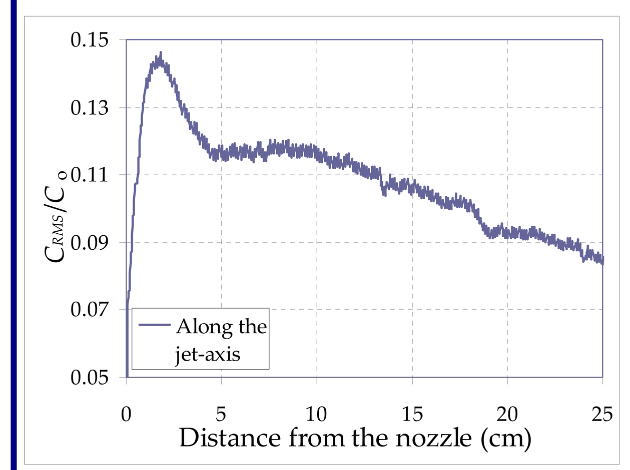

Figure 6a: Distribution of the RMS concentration along the jet-axis.

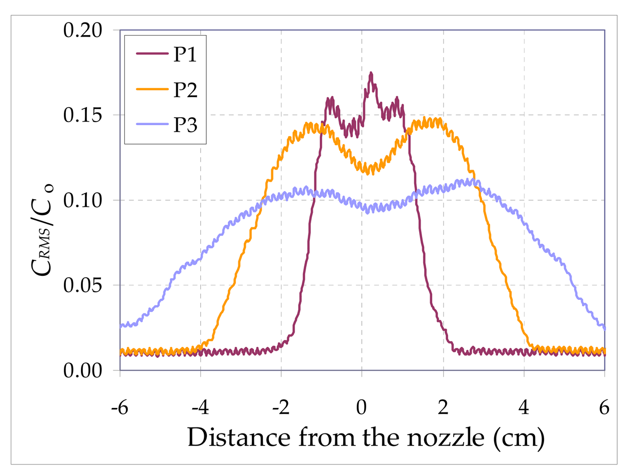

Figure 6b: Distribution of the RMS concentration perpendicular to the jet-axis.

On the right figure the total noise caused by artificial sources seem to be very low. Also, one can observe the sudden increase of the RMS (this is the end of ZFE).

The maximum RMS value is ≈0.15. Also, the two humps of the SDD on the right figure are a trace of the two RMS axes as they develop at the boundaries of the jet. These observations are also experimentally verified with Papanicalou &List (1987) ones.

5. Temporal CDF and PDF

The estimated temporal CFD and PDF of the concentration are described and presented here.

$CPF \equiv P(C_m \le c_m) = E\{N(C_m \le c_m)/N_o\}$, where

P is for probability, $E\{...\}$ is the notation for the expected value,

C_m defines the concentration field (where its mean value has been abstracted),

$N(C_m \le c_m)$ is the number of concentrations less or equal to a value c_m and

N_o is the total number of records.

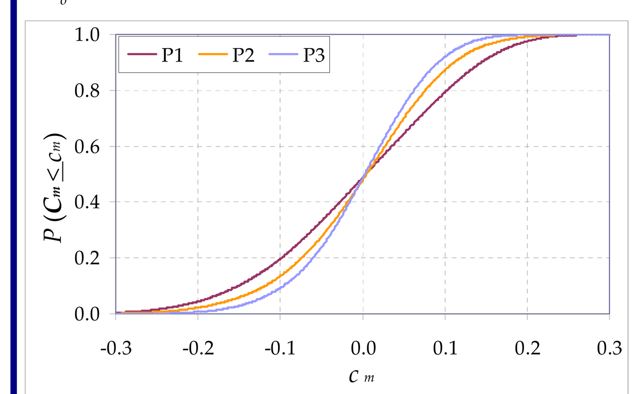

Figure 7a: Distribution of the concentration along the jet-axis.

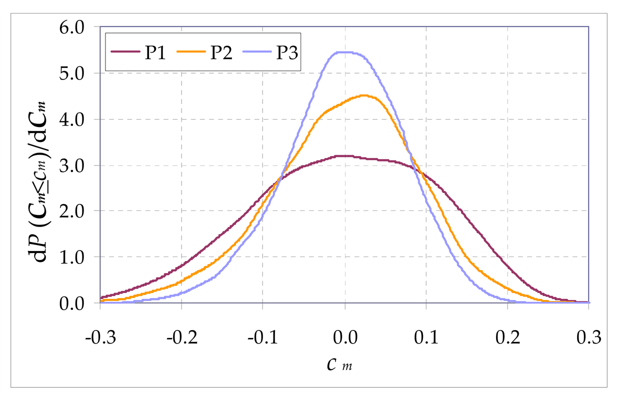

Figure 7b: Distribution of the concentration perpendicular to the jet-axis.

Again the temporal CDF and PDF seem to approximate the log-normal one. Also, the PDFs show a small assymetry, probably due to small motion of ambient water.

6. Energy spectrum

The estimated ES of the concentration are presented below. All ES have been smoothed according to Welch's method (with no overlapping segments). A raw ES is also shown for comparison with the corresponding smoothed one. The ES are calculated using the equation below:

$E_s(w) \overset{T\to\infty}{=} |F(w)|^2 / T$, where

$F(w) = \int_{-\infty}^{+\infty} S(t)\, e^{-2\pi wri}\, dr$, the Fourier transform of the concentration timeseries and

t is the time vector (sec), T the total duration of the timeseries (sec) and w the frequency (Hz).

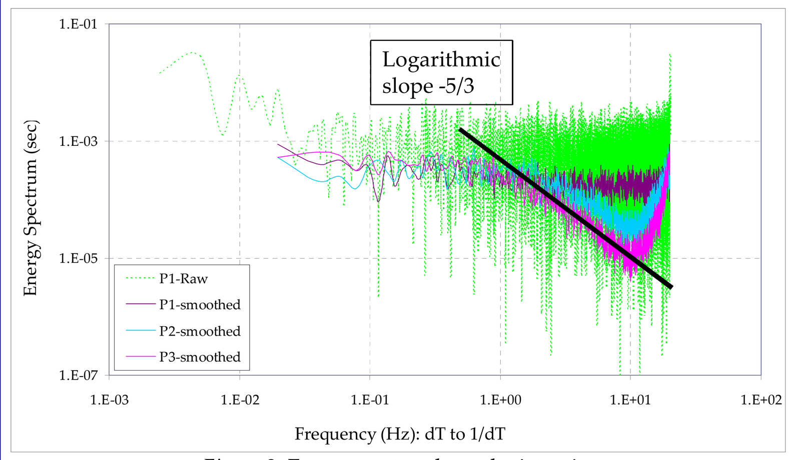

Figure 8: Energy sectra along the jet-axis.

Kolmogorov logarithmic slope (indicating the turbulent energy dissipation rate) in the inertial area of scales, approximates the log-slope of the smoothed ES of the most remote measured point (P3). There, the turbulent eddies are of larger scales and smaller frequencies and thus, possible to trace with this experiment's recording speed.

Moreover, one can comment on the great difference the raw and smoothed ES have.

7. Climacograms and Hurst-Kolmogorov coefficient

The Cl is a logarithmic plot of the standard deviation (SD) of the mean-aggregated series versus the aggregated scale (k) (Koutsoyiannis, 2011). The HKc is the logarithmic slope of the Cl as scale tends to infinity and it used to quantify the long term change (or else memory, persistence, clustering) of the process. For 0<HKc<0.5 the process is anticorrelated (ACF<0), for 0.5<HKc<1 the process is correlated and for HKc=0.5 the process is purely random. The estimated (for the C_m timeseries) Cl and HKc are presented below.

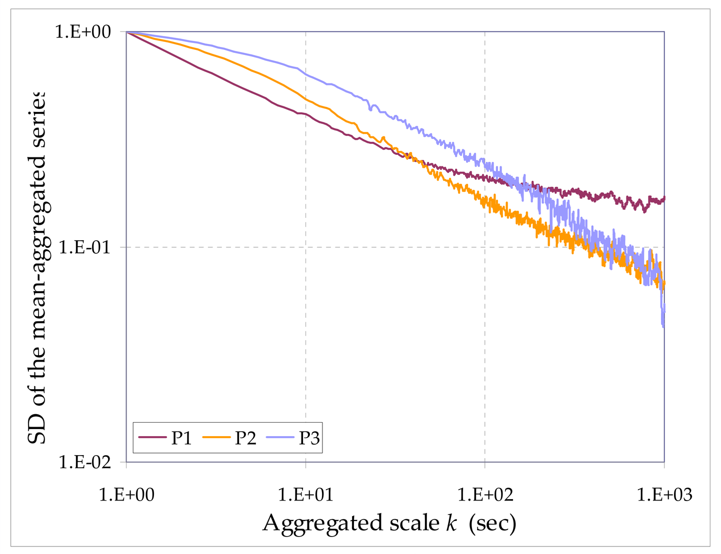

Figure 9: Climacograms along the jet-axis.

The HKc is found here to be around 0.9, 0.8 and 0.7 for P1, P2 and P3. Note, that bias is not included (assuming i.e. an HK model).

Close to the area of the nozzle (but outside the ZFE) one would expect a white noise behavior (HKc≈0.5) and away from the nozzle (in the plume-like area, where Si/lm>>1) a much more larger HKc. Here, all the points lie within the jet-like area. It is observed that the HKc is decreasing as moving away from the nozzle. This behavior is similar to the one Dimitriadis &Papanicolaou (2010) observed and maybe is due to instabilities occurring at the jet-like area.

8. Autocorrelations and Structural function of 2nd order

ACF(s) = $E\{C_m(t)\ C_m(t+s)\}$/ACF(0) and S2F(s)=1-ACF(s), assuming a stationary process, where the functions depend only on the time-lag s (sec).

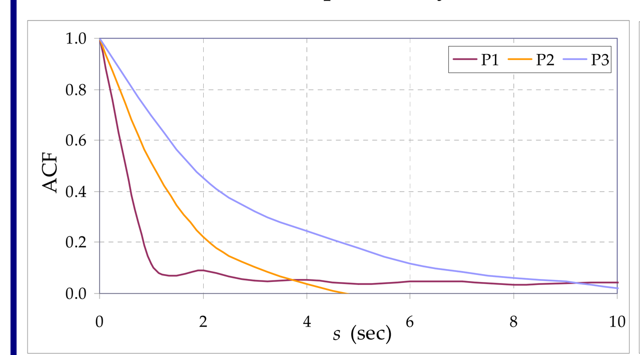

Figure 10a: ACF along the jet-axis.

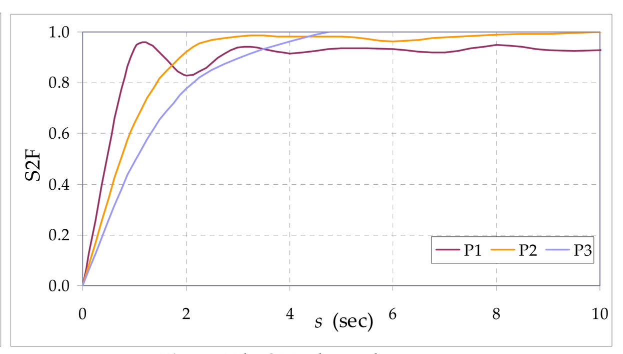

Figure 10b: S2F along the jet-axis.

The estimated ACF and S2F are presented above. The ACF is decreasing much faster as moving away from the nozzle which comes in agreement with the decreasing of the specific momentum flux and thus, the random noise behavior.

References

- Dimitriadis P. & Papanicolaou, P., 'Hurst-Kolmogorov dynamics applied to temperature field of horizontal turbulent buoyant jets', *EGU General Assembly*, Vol. 12, EGU2010-10644, 2010.
- Ferrier A.J., Funk D.R., and Roberts P.J.W.. 'Application of optical techniques to the study of plumes in stratified fluids', *Dynamics of Atmospheres and Oceans*, Vol. 20, pp. 155-183, 1993.
- Koutsoyiannis, D., 'Hurst-Kolmogorov dynamics and uncertainty,' *Journal of the American Water Resources Association*, Vol. 47 (3), 481–495, 2011.
- Papanicolaou P.N. & List E.J., 'Statistical and spectral properties of tracer concentration in round buoyant jets', *Int. J. Heat Mass Transfer,* Vol. 30(10), 2057-2071, 1987.
- Walker D.A., 'A Fluorescence Technique for Measurement of Concentration in Mixing Liquids', *J. Phys E: Sci Instrum,* Vol. 20, pp.217–224A, 1987.